Tumbling of small axisymmetric particles in random and turbulent flows

K. Gustavsson, J. Einarsson, and B. Mehlig
Department of Physics, Gothenburg University, 41296 Gothenburg, Sweden

We analyse the tumbling of small non-spherical, axisymmetric particles in random and turbulent flows. We compute the orientational dynamics in terms of a perturbation expansion in the Kubo number, and obtain the tumbling rate in terms of Lagrangian correlation functions. These capture preferential sampling of the fluid gradients which in turn can give rise to differences in the tumbling rates of disks and rods. We show that this is a weak effect in Gaussian random flows. But in turbulent flows persistent regions of high vorticity cause disks to tumble much faster than rods, as observed in direct numerical simulations [Parsa *et al.*, Phys. Rev. Lett. **109** (2012) 134501]. For larger particles (at finite Stokes numbers), rotational and translational inertia affects the tumbling rate and the angle at which particles collide, due to the formation of rotational caustics.

The orientational dynamics of axisymmetric particles in random and turbulent flows is of great significance in many areas of the Natural Sciences and in technology. Tumbling and rotation of small non-spherical particles is of fundamental interest because it reflects the statistics of the velocity gradients in turbulent flows [1]. The dynamics of fibre suspensions is of interest in industrial applications [2]. Patterns of non-spherical particles suspended in random flows were investigated in [3–5], revealing singularities in the orientational patterns of rheoscopic suspensions. Aerosols in the natural world are often suspensions of non-spherical particles: tumbling ice particles in turbulent clouds may play an important role in cloud-particle interactions [6]. Dust grains in circumstellar accretion disks are not spherically symmetric [7] and the relative orientation at which such grains collide may have important consequences for the outcome of the collision process. Moreover, rotation affects the magnitude of photophoretic forces on the particles [8]. Finally, tumbling may allow rod-like plankton in the ocean to sweep up nutrients more efficiently [9]. Recently, the tumbling rate of small axisymmetric particles in turbulent flows was investigated experimentally and by means of direct numerical simulations [10]. It was found that disks tumble, on average, at a much higher rate than rods. This was related to the observation that rods tend to preferentially align with the vorticity of the flow [11].

The equations of motion for disks and rods are almost the same, the only difference is that the flow-gradient matrix for rods is replaced by its negative transpose for disks. In Gaussian random flows one may thus expect the difference in tumbling rate between disks and rods to be negligible. This raises the questions: How does the tumbling in turbulent flows differ from that in random flows, and which mechanisms are responsible? How sensitive is the orientational dynamics to differences between random and turbulent flows? How does the nature of the Lagrangian flow statistics influence the tumbling? How does tumbling reflect vorticity? Finally, what is the effect of particle inertia upon the tumbling?

To answer these questions we analyse the tumbling of small non-spherical particles in random and turbulent flows using perturbation theory. We show how in the absence of inertia, tumbling in turbulent and random flows is determined, to leading order, by Lagrangian 3-point correlations of the fluid gradients. We compute these correlations in random flows and show that preferential effects exist but are small. In turbulent flows we evaluate the correlation functions numerically, using the JHU turbulence data set [12, 13]. We find that they give rise to a substantial difference in the tumbling rate between rods and disks. We explain this difference by the fact that persistent regions of high vorticity strongly contribute to the Lagrangian three-point statistics. In low-vorticity regions of the flow, by contrast, disks and rods tumble on average at similar rates. At finite values of St rotational and translational inertia of the particles affects the tumbling rate and the angle at which particles collide, due to the formation of rotational caustics.

The dynamics of small axisymmetric particles in a flow is governed, in the simplest model, by three dimensionless parameters. The Kubo number $\mathrm{Ku} = u_0\tau/\eta$ is a dimensionless measure of the correlation time of the flow, here u_0, τ and η are the smallest characteristic speed-, time- and length scales of the flow (Kolmogorov scales in turbulence). The Stokes number $(\gamma\tau)^{-1}$ characterises the damping of the particle dynamics with respect to the flow. Here γ is the Stokes damping constant. Third, λ is the aspect ratio of the axisymmetric particle.

In the limit of St $\to 0$, centre-of-mass and orientational dynamics decouple. The centre-of-mass $\boldsymbol{r}$ is simply advected. The orientational dynamics of the unit vector $\boldsymbol{n}$ pointing along the symmetry axis of the particle is driven by the local flow gradients (provided that the dimensions of the particle are much smaller than η). In other words $\boldsymbol{n}$ follows Jeffery's equation [14]. In the following we use dimensionless units $t = \tau t'$, $\boldsymbol{r} = \eta \boldsymbol{r}'$, $\boldsymbol{u} = u_0 \boldsymbol{u}'$. Dropping the primes, the equation of motion reads:

$$\dot{\boldsymbol{r}} = \mathrm{Ku}\,\boldsymbol{u}\,, \quad \dot{\boldsymbol{n}} = \mathrm{Ku}\left[\mathbb{O}\boldsymbol{n} + \Lambda\left(\mathbb{S}\boldsymbol{n} - (\boldsymbol{n}^{\mathrm{T}}\mathbb{S}\boldsymbol{n})\boldsymbol{n}\right)\right]\,. \quad (1)$$

Here $\Lambda = (\lambda^2 - 1)/(\lambda^2 + 1)$ parameterises the particle shape ($\Lambda = -1$ for disks, 0 for spheres, and 1 for rods). Further $\mathbb{S} = (\mathbb{A} + \mathbb{A}^{\mathrm{T}})/2$ and $\mathbb{O} = (\mathbb{A} - \mathbb{A}^{\mathrm{T}})/2$ are the symmetric and antisymmetric parts of the matrix $\mathbb{A}(\boldsymbol{r}, t)$ of flow gradients. The time-averaged tumbling rate $\langle \dot{n}^2 \rangle$ is determined by the fluctuations of $\mathbb{S}(\boldsymbol{r}_t, t)$ and $\mathbb{O}(\boldsymbol{r}_t, t)$ along the particle trajectories $\boldsymbol{r}_t \equiv \boldsymbol{r}(t)$ (corresponding to Lagrangian statistics at St = 0). In the limit of rapidly fluctuating random flows (Ku $\to$ 0) the rate averaged along trajectories can be replaced by an average over the ensemble of $\mathbb{S}$ and $\mathbb{O}$. We denote this average by $\langle \dot{n}^2 \rangle_0$. It is determined by the invariants of the matrices $\mathbb{S}$ and $\mathbb{O}$. For incompressible, isotropic random flows one finds:

$$\langle \dot{n}^2 \rangle \approx \langle \dot{n}^2 \rangle_0 = \mathrm{Ku}^2 \big(-5\mathrm{Tr}\langle \mathbb{O}^2 \rangle + 3\Lambda^2 \mathrm{Tr}\langle \mathbb{S}^2 \rangle \big)/15\,. \quad (2)$$

Note that in homogenous flows $\mathrm{Tr}\langle \mathbb{S}^2 \rangle = -\mathrm{Tr}\langle \mathbb{O}^2 \rangle = \mathrm{Tr}\langle \mathbb{A}^{\mathrm{T}}\mathbb{A} \rangle/2$. In turbulent flows $\mathrm{Tr}\langle \mathbb{A}^{\mathrm{T}}\mathbb{A} \rangle$ is proportional to the energy dissipation. An expression equivalent to (2) was first derived in [15] and is also quoted in [10]. Since Eq. (2) is symmetric in Λ, disks tumble at the same rates as rods. Differences between disks and rods could arise for two reasons. First, one or more symmetries may be broken. Breaking for example isotropy gives rise to an extra term that is odd in Λ. This is the case in the flow studied in [16]. Second, in homogenous, isotropic, and incompressible flows differences in the behaviour of disks and rods may arise due to preferential sampling of the flow gradients.

In order to understand and quantify such effects it is necessary to evaluate the Lagrangian statistics of $\mathbb{S}(\boldsymbol{r}_t, t)$ and $\mathbb{O}(\boldsymbol{r}_t, t)$ at finite values of Ku. This is possible by iterating the implicit solution of (1):

$$\boldsymbol{n}_{t'} = \boldsymbol{n}_0 + \mathrm{Ku}\int_0^{t'}\mathrm{d}t\,[\mathbb{O}_t \boldsymbol{n}_t + \Lambda(\mathbb{S}_t \boldsymbol{n}_t - (\boldsymbol{n}_t^{\mathrm{T}}\mathbb{S}_t \boldsymbol{n}_t)\boldsymbol{n}_t)]\,, \quad (3)$$

where $\mathbb{O}_t \equiv \mathbb{O}(\boldsymbol{r}_t, t)$ and $\mathbb{S}_t \equiv \mathbb{S}(\boldsymbol{r}_t, t)$. Iteratively substituting $\boldsymbol{n}_t$ into the r.h.s. of (3) generates perturbation expansions for $\boldsymbol{n}_t$ and its time derivative in powers of Ku. Averaging over the ensemble of flow gradients and over the initial flow configuration (equivalent to taking $t \to \infty$) we find the leading-order correction to Eq. (2)

$$\langle \dot{n}^2 \rangle = \langle \dot{n}^2 \rangle_0 + \frac{2}{5}\mathrm{Ku}^3 \Lambda \int_0^\infty \mathrm{d}t \quad (4)$$
$$\times \big[-\mathrm{Tr}\langle \mathbb{O}_0^2 \mathbb{S}_{-t} \rangle + 2\Lambda\mathrm{Tr}\langle \mathbb{S}_0 \mathbb{O}_0 \mathbb{S}_{-t} \rangle + \frac{3}{7}\Lambda^2 \mathrm{Tr}\langle \mathbb{S}_0^2 \mathbb{S}_{-t} \rangle \big]\,.$$

This correction is given by three-point Lagrangian correlation functions of $\mathbb{O}_t$ and $\mathbb{S}_t$. We have used the fact that two- and three-point correlation functions between $\mathbb{O}$ and $\mathbb{S}$ in isotropic and incompressible flows separate as follows:

$$\langle S_{ij,0}S_{kl,t} \rangle = \mathrm{Tr}\langle \mathbb{S}_0 \mathbb{S}_t \rangle F_{ijkl}^{SS}\,,$$
$$\langle O_{ij,0}O_{kl,t} \rangle = \mathrm{Tr}\langle \mathbb{O}_0 \mathbb{O}_t \rangle F_{ijkl}^{OO}\,, \quad \langle O_{ij,0}S_{kl,t} \rangle = 0\,, \quad (5)$$
$$\langle O_{ij,0}O_{kl,t}S_{mn,t'} \rangle = \mathrm{Tr}\langle \mathbb{O}_0 \mathbb{O}_t \mathbb{S}_{t'} \rangle F_{ijklmn}^{OOS}\,,$$
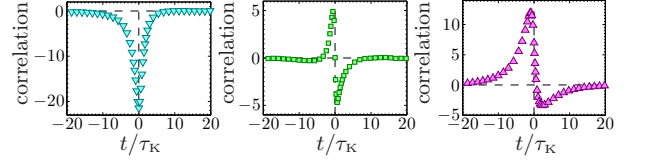

FIG. 1: *(Color online).* Numerical results for Lagrangian correlations $\mathrm{Tr}\langle \mathbb{S}_0^2 \mathbb{S}_t \rangle \tau_{\mathrm{K}}^3$ (cyan,$\triangledown$), $\langle \mathrm{Tr}\mathbb{S}_0 \mathbb{O}_0 \mathbb{S}_t \rangle \tau_{\mathrm{K}}^3$ (green,$\square$) and $\mathrm{Tr}\langle \mathbb{O}_0^2 \mathbb{S}_t \rangle \tau_{\mathrm{K}}^3$ (magenta,$\triangle$). Obtained using the JHU turbulence data set [12, 13], see text. In units of $\tau_{\mathrm{K}} \equiv 1/\sqrt{\mathrm{Tr}\langle \mathbb{A}^{\mathrm{T}}\mathbb{A} \rangle}$.

and so forth. The tensors F_{ijkl}^{SS}, … are combinations of products of Kronecker deltas determined by the symmetries of the flow (incompressibility and isotropy).

Eq. (4) shows that the Ku^3-correction to (2) contains terms antisymmetric in Λ, causing disks to tumble differently from rods. For Gaussian random flows, the Lagrangian correlation functions in the integrands of (4) can be calculated analytically for small Ku, as we show below. For turbulent flows we have determined the correlation functions numerically, using data from the JHU turbulence data set [12, 13].

Random flows. We represent the incompressible, homogenous, and isotropic random flow as $\boldsymbol{u}(\boldsymbol{r}, t) = \nabla \wedge \boldsymbol{A}(\boldsymbol{r}, t)$ in terms of a Gaussian random vector potential $\boldsymbol{A}(\boldsymbol{r}, t)$ with zero mean and correlation function [17]

$$\langle A_i(\boldsymbol{r}_0, 0)A_j(\boldsymbol{r}_0, t) \rangle = \delta_{ij}\exp(-|t|)/6\,. \quad (6)$$

The corresponding Eulerian correlation functions (evaluated at a fixed point in space) are given by $\mathrm{Tr}\langle \mathbb{S}(\boldsymbol{r}_0, 0)\mathbb{S}(\boldsymbol{r}_0, t) \rangle = -\mathrm{Tr}\langle \mathbb{O}(\boldsymbol{r}_0, 0)\mathbb{O}(\boldsymbol{r}_0, t) \rangle = 5\,e^{-|t|}/2$. The Eulerian three-point functions vanish because the Gaussian gradient distribution is symmetric. The Lagrangian correlations at finite values of Ku can be computed systematically with a perturbation expansion taking into account recursively that the actual trajectory $\boldsymbol{r}_t$ deviates from its initial condition $\boldsymbol{r}_0$. As shown in [18, 19] this yields an expansion in Ku that gives accurate steady-state results provided that the deviations within a correlation time τ of the flow are smaller than the correlation length η.

The Lagrangian correlation functions quantify the degree of preferential sampling. We illustrate this by the lowest-order result for Lagrangian two-point correlations:

$$\mathrm{Tr}\langle \mathbb{S}_0 \mathbb{S}_t \rangle = \frac{5}{2}e^{-|t|}\big[1 + \frac{17\mathrm{Ku}^2}{6}\big(1 - |t| - e^{-|t|}\big)\big]\,, \quad (7)$$
$$\mathrm{Tr}\langle \mathbb{O}_0 \mathbb{O}_t \rangle = -\frac{5}{2}e^{-|t|}\big[1 + \frac{3\mathrm{Ku}^2}{2}\big(1 - |t| - e^{-|t|}\big)\big]\,.$$

We see that the Lagrangian correlations of $\mathbb{S}(\boldsymbol{r}_t, t)$ differ from those of $\mathbb{O}(\boldsymbol{r}_t, t)$, they decay faster, and they both decay more rapidly than $\exp(-|t|)$. This is simply due to the fact that straining regions in the flow make large contributions to the correlation of $\mathbb{S}$, but particles

2

in straining regions are more quickly displaced than particles in rotating regions.

Differences in tumbling rates between disks and rods are determined by Lagrangian three-point correlations. We find to third order in Ku:

$$\text{Tr}\langle \mathbb{S}_0 \mathbb{O}_0 \mathbb{S}_t \rangle = \frac{35\text{Ku}^3}{16}\text{sgn}(t)e^{-|t|}(1-2|t|e^{-|t|}-e^{-2|t|}),$$

$$\text{Tr}\langle \mathbb{O}_0 \mathbb{O}_0 \mathbb{S}_t \rangle = -\frac{125\text{Ku}^3}{288}\text{sgn}(t)e^{-|t|}(1-2|t|e^{-|t|}-e^{-2|t|}),$$

$$\text{Tr}\langle \mathbb{S}_0^2 \mathbb{S}_t \rangle = -\frac{175\text{Ku}^3}{96}\text{sgn}(t)e^{-|t|}(1-2|t|e^{-|t|}-e^{-2|t|}). \quad (8)$$

We infer that the Lagrangian fluctuations of the flow gradient are non-Gaussian, a consequence of preferential sampling at finite Kubo numbers.

Inserting Eq. (8) into (4) we obtain:

$$\langle \dot{n}^2 \rangle = \frac{\text{Ku}^2}{6}(5+3\Lambda^2) - \frac{\text{Ku}^4}{4}\Lambda^2(5+3\Lambda^2) \quad (9)$$

$$+ \frac{\text{Ku}^6}{864}\Lambda(-25+4668\Lambda+45\Lambda^2+7236\Lambda^3+2484\Lambda^5)+\dots.$$

We see that odd powers in Λ occur in this expression, giving rise to differences in tumbling between disks and rods. But the effect is weak, it occurs to order Ku^6. We conclude that disks and rods tumble at almost the same rates in Gaussian random flows. The question is thus what causes the striking differences between the dynamics of rods and disks observed in [10]?

Turbulent flows. According to Eq. (4) differences in the tumbling of rods and disks to preferential sampling of the flow gradients are parameterised by Lagrangian three-point correlation functions. We cannot compute these correlation functions analytically, and have thus evaluated them numerically using the JHU turbulence data set [12, 13]. The data set contains a direct numerical simulation of forced, isotropic turbulence on a 1024^3 grid, for circa 45 Kolmogorov times, at a Taylor microscale Reynolds number $\text{Re}_\lambda = 433$. From the data set we computed the Lagrangian correlations. We checked that they factorised according to Eq. (5). The three correlation functions contributing to the tumbling rate in Eq. (4) are shown in Fig. 1. The major contribution after integration comes from the $\text{Tr}\langle \mathbb{O}_0^2 \mathbb{S}_{-t} \rangle$-term, with the contribution of the $\text{Tr}\langle \mathbb{S}_0^2 \mathbb{S}_{-t} \rangle$-term approximately a factor $\Lambda^2/3$ smaller. These two terms together result in a substantial contribution to the tumbling rate that is odd in Λ, giving rise to pronounced differences in the tumbling of rods and disks. Which particular structures in the turbulent flow, not present in random flows, cause this effect?

The dynamics of disks and rods is closely related. Taking the limits $\lambda \to 0$ and $\lambda \to \infty$ in Eq. (1) shows that the unnormalised orientation vectors $\boldsymbol{q}$ (such that $\boldsymbol{n} = \boldsymbol{q}/|\boldsymbol{q}|$) of disks and rods obey $\dot{\boldsymbol{q}}_{\text{disk}} = -\mathbb{A}^{\text{T}}\boldsymbol{q}_{\text{disk}}$ and $\dot{\boldsymbol{q}}_{\text{rod}} = \mathbb{A}\boldsymbol{q}_{\text{rod}}$. Differences in the dynamics of rods and disks arise in regions where the flow persists for long enough so that $\boldsymbol{q}$ has

time to align with the eigenvectors of $\mathbb{A}$ or of $-\mathbb{A}^{\text{T}}$. The eigenvectors of $\mathbb{A}$ and $-\mathbb{A}^{\text{T}}$ are related: denote the eigenvectors of $\mathbb{A}$ by $\boldsymbol{R}_i$ for $i = 1,\dots,3$ with corresponding maximal eigenvalue for $i = 1$ and minimal eigenvalue for $i = 3$. Those of $\mathbb{A}^{\text{T}}$ are given by $\boldsymbol{L}_1 = \boldsymbol{R}_2 \wedge \boldsymbol{R}_3$ with cyclic permutations of the indices. In incompressible flows the eigensystem of $\mathbb{A}$ is classified by the invariants $\text{Tr}\mathbb{A}^2$ and $\text{Tr}\mathbb{A}^3$ [20], and there are three possibilities. First when $\text{Tr}\mathbb{A}^2$ is large enough, then all eigenvalues of $\mathbb{A}$ are real, and rods align with $\boldsymbol{R}_1$ while disks align with $\boldsymbol{L}_3$. When by contrast $\text{Tr}\mathbb{A}^2$ is not large, then the two remaining possibilities are. Second when $\text{Tr}\mathbb{A}^3 > 0$, then the maximal eigenvalue of $\mathbb{A}$ is real, and the minor eigenvalues are complex conjugates. In this case rods align with $\boldsymbol{R}_1$, while disks rotate in the plane orthogonal to $\boldsymbol{R}_1$. Third, when $\text{Tr}\mathbb{A}^3 < 0$, the two major eigenvalues of $\mathbb{A}$ are complex conjugates and the minor eigenvalue is real. In this case the rod rotates in the plane orthogonal to $\boldsymbol{L}_3$ while the disk aligns with $\boldsymbol{L}_3$.

This apparent symmetry in the dynamics of rods and disks in persistent flows (corresponding to $\text{Tr}\mathbb{A}^3 \leftrightarrow -\text{Tr}\mathbb{A}^3$) is broken in turbulence: the joint distribution of $\text{Tr}\mathbb{A}^2$ and $\text{Tr}\mathbb{A}^3$ is strongly skewed [21]. This explains why rods and disks tumble differently in persistent flow regions - but not in general.

While the argument in the previous paragraph relies on a picture valid for persistent flows, or at large Ku, Eq. (4) was derived using a small-Ku expansion. We now show that the conclusions drawn from the previous paragraph and from Eq. (4) are in fact closely connected. To this end we decompose $\text{Tr}\mathbb{A}^2 = \text{Tr}\mathbb{S}^2 + \text{Tr}\mathbb{O}^2$ and $\text{Tr}\mathbb{A}^3 = 3\text{Tr}\mathbb{O}^2\mathbb{S} + \text{Tr}\mathbb{S}^3$. where $\text{Tr}\mathbb{S}^2 \geq 0$ and $\text{Tr}\mathbb{O}^2 \leq 0$. On average $\text{Tr}\langle \mathbb{O}^2\mathbb{S} \rangle > 0$ and $\text{Tr}\langle \mathbb{S}^3 \rangle < 0$ (see Fig. 1). Thus large positive values of $\text{Tr}\mathbb{A}^3$ typically correspond to large values of $\text{Tr}\mathbb{O}^2\mathbb{S}$ which typically imply large negative values of $\text{Tr}\mathbb{O}^2$. Regions with large $\text{Tr}\mathbb{O}^2\mathbb{S}$ correspond to vortex tubes [22] that persist long enough for rods to align and disks to tumble (case (b) discussed above). This finding corresponds to the conclusions drawn from Eq. (4), namely that differences in the tumbling rates of disks and rods are due to regions where $\text{Tr}\,\mathbb{O}_0^2\mathbb{S}_{-t}$ persists long enough to make a substantial contribution to $\langle \dot{n}^2 \rangle$. Conversely, large negative values of $\text{Tr}\mathbb{A}^3$ typically correspond to large negative values of $\text{Tr}\mathbb{S}^3$ which typically implies large positive values of $\text{Tr}\mathbb{S}^2$. This region corresponds to case (a) discussed above, and is reflected in the integral over $\text{Tr}\mathbb{S}_0^2\mathbb{S}_{-t}$ in Eq. (4). In this region the reason for the difference in tumbling rate between rods and disks is due to the difference in magnitude of eigenvalues. Since the middle eigenvalue of $\mathbb{A}$ is positive on average, and the sum of eigenvalues is zero in an incompressible flow, the magnitude of the first eigenvalue (acting on the rod) is necessarily smaller than that of the last (acting on the disk). We thus expect disks to respond more quickly than rods to persistent regions of type (a) and hence exhibit a larger tumbling rate in such regions.
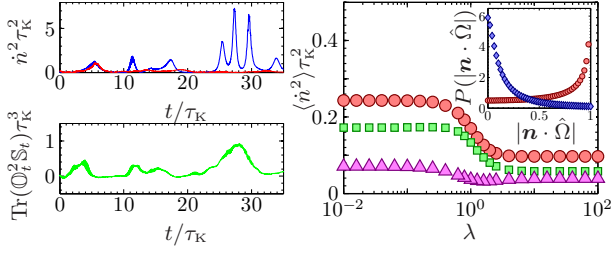
FIG. 2: *(Color online)*. Left: Tumbling rate $\dot{n}^2$ for a disk (blue) and a rod (red) in turbulent flow as a function of time, using the JHU turbulence data set [12, 13]. Also shown is $\mathrm{Tr}\,\mathbb{O}_t^2 \mathbb{S}_t$ (green). Right: average squared tumbling rate $\langle \dot{n}^2 \rangle$ in turbulence as a function of the aspect ratio λ (red,$\circ$). Also shown is $\dot{n}^2$ averaged conditional on large values of $\mathrm{Tr}\,\mathbb{O}_t^2 \mathbb{S}_t$ (green,$\square$) (23% of the sampled data) conditional on small values of $\mathrm{Tr}\,\mathbb{O}_t^2 \mathbb{S}_t$ (magenta,$\triangle$) (77% of the sampled data). Inset: alignment distributions for disks (blue,$\diamond$) and rods (red,$\circ$).

FIG. 3: *(Color online)*. Left: $\langle \dot{n}^2 \rangle$ as a function of St in a Gaussian random flow (see text). Symbols show results of numerical simulations, solid lines show theory (11). Parameters: $\mathrm{Ku} = 0.1$, $\lambda = \sqrt{0.1}$ (blue,$\diamond$), $\lambda = 1$ (green,$\square$), $\lambda = \sqrt{10}$ (red,$\circ$). Right: distribution of the relative angle $\Delta\varphi$ between the orientation vectors $\boldsymbol{n}$ of two particles close together (at separation $R = 0.1\eta$). Parameters: $\mathrm{Ku} = 1$, $\lambda = \sqrt{10}$. St $= 0$ (cyan, $\triangledown$), St $= 1$ (green, $\square$) and St $= 10$ (magenta, $\triangle$).

Fig. 2 (left) shows how $\dot{n}^2$ varies as a function of time in a turbulent flow $\boldsymbol{u}(\boldsymbol{r}, t)$ (taken from [12, 13]). Also shown is $\mathrm{Tr}\,\mathbb{O}_t^2 \mathbb{S}_t$. In agreement with the calculations and arguments outlined above, rods align and disks tumble strongly when $\mathrm{Tr}\,\mathbb{O}_t^2 \mathbb{S}_t$ is large. Fig. 2 (right) shows numerical results for $\langle \dot{n}^2 \rangle$ in a turbulent flow, as a function of the aspect ratio λ. Also shown is $\dot{n}^2$ averageed conditional on large $\mathrm{Tr}\,\mathbb{O}_t^2 \mathbb{S}_t$: the substantial difference in tumbling rates of disks and rods is largely caused by the flow configurations with large $\mathrm{Tr}\,\mathbb{O}_t^2 \mathbb{S}_t$, confirming the picture outlined above.

Finally we note that when rods align with $\boldsymbol{R}_1$, then the vorticity vector $\boldsymbol{\Omega} = (\boldsymbol{\nabla} \wedge \boldsymbol{u})/2$ also aligns with $\boldsymbol{R}_1$, while the for disks $\boldsymbol{n}$ is preferentially orthogonal to $\boldsymbol{\Omega}$ (inset of right panel of Fig. 2). This is expected since the equations of motion for rods and vorticity have a common term involving $\mathbb{A}$ [1, 11].

Effects of particle inertia. When St > 0, the centre-of-mass motion no longer decouples from the orientational dynamics of the particle. Different moments of inertia and fluid resistance tensors result in differences in the tumbling of disks and rods at finite St. Neglecting possible effects due to the unsteadiness of the flow, the dynamics of small axisymmetric particles at finite St is

$$\dot{\boldsymbol{r}} = \mathrm{Ku}\,\boldsymbol{v}\,, \qquad \mathrm{St}\,\dot{\boldsymbol{v}} = \mathbb{M}\,(\boldsymbol{u} - \boldsymbol{v}) \qquad (10)$$

$$\dot{\boldsymbol{n}} = \mathrm{Ku}\,\boldsymbol{\omega} \wedge \boldsymbol{n}\,, \; \mathrm{St}\,(\mathbb{I}\dot{\boldsymbol{\omega}}) = \mathbb{D}\,(\boldsymbol{\Omega} - \boldsymbol{\omega}) + \mathbb{H}\!:\!\mathbb{S}$$

Here $\boldsymbol{v}$ and $\boldsymbol{\omega}$ are particle velocity and angular velocity, $\mathbb{I}$ is the inertia tensor of the particle, $\mathbb{M}, \mathbb{D}$ and $\mathbb{H}$ are Brenner's resistance tensors [23], and $\mathbb{H}\!:\!\mathbb{S}$ denotes contraction over two indices. Finally, $\boldsymbol{T} = \mathbb{D}\,(\boldsymbol{\Omega} - \boldsymbol{\omega}) + \mathbb{H}\!:\!\mathbb{S}$ is Jeffery's torque [14]. In the limit St $\to 0$, Eq. (1) is recovered.

The tumbling rate resulting from the corresponding equation of motion can be computed in a small-Ku perturbation theory, analogous to our treatment of Eq. (1) outlined above. To lowest order in Ku we find for a spheroid in the random-flow model:
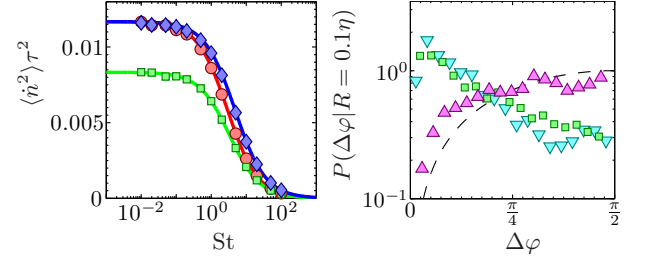
$$\langle \dot{n}^2 \rangle = \frac{\mathrm{Ku}^2}{6} \frac{C_\perp^{(r)}\,(5 + 3\Lambda^2)}{\mathrm{St} + C_\perp^{(r)}}\,, \; C_\perp^{(r)} = \frac{40(\lambda^2 - 1)}{9\lambda((2\lambda^2 - 1)\beta - 1)}\,,$$

$$\beta = \frac{1}{\lambda\sqrt{|\lambda^2 - 1|}} \begin{cases} \mathrm{acos}(\lambda) & \text{if } \lambda \leq 1 \\ \mathrm{acosh}(\lambda) & \text{if } \lambda > 1 \end{cases}\,. \qquad (11)$$

The result (11) is shown in Fig. 3 in comparison with results of numerical simulations. We see that the tumbling rate decreases as St increases. This is due to the fact that the coupling to the flow weakens as St increases. To order Ku^2 the tumbling rates of disks and rods coincide in the limit of St $\to 0$ in agreement with (2). But at finite Stokes numbers differences in the moments of inertia and fluid resistance tensors of disks and rods result in differences in the orientational dynamics.

At finite Stokes numbers the centre-of-mass motion of inertial particles exhibit caustics where the phase-space manifold describing the dependence of centre-of-mass velocity upon position folds over giving rise to large velocity differences between close-by particles. For non-spherical particles phase space contains angular degrees of freedom. In this case caustics cause particles with misaligned orientation vectors to collide. Fig. 3 (right) shows the distribution of angles $\Delta\varphi$ between orientation vectors of nearby particles. At larger values of St caustics occur more frequently, giving rise to a broader distribution of the collision angle $\Delta\varphi$. At still larger St the distribution approaches that between uniformly randomly distributed unit vectors, $P(\Delta\varphi) = \sin \Delta\varphi$.

[1] A. Pumir and M. Wilkinson, NJP **13**, 093030 (2011).
[2] F. Lundell, D. Söderberg, and H. Alfredsson, Annu. Rev. Fluid Mech. **43**, 195 (2011).
[3] M. Wilkinson, V. Bezuglyy, and B. Mehlig, Phys. Fluids **21**, 043304 (2009).
[4] V. Bezuglyy, B. Mehlig, and M. Wilkinson, Europhys. Lett.) **89**, 34003 (2010).
[5] M. Wilkinson, V. Bezuglyy, and B. Mehlig, J. Fluid Mech. **667**, 158 (2011).
[6] H. R. Pruppacher and J. D. Klett, *Microphysics of Clouds and Precipitation* (Springer, 1997).
[7] G. Praburam and J. Goree, Astrophys. J. **441**, 830 (1995).
[8] J. van Eymeren and G. Wurm, Monthly Notices of the Royal Astronomical Society **420**, 183 (2012).
[9] J. S. Guasto, R. Rusconi, and R. Stocker, Annual Review of Fluid Mechanics **44**, 373 (2012).
[10] S. Parsa, E. Calzavarini, F. Toschi, and G. A. Voth, Phys. Rev. Lett. **109**, 134501 (2012).
[11] M. Wilkinson and H. Kennard, J. Phys. A **45**, 455502 (2012).
[12] Y. Li, E. Perlman, M. Wan, Y. Yang, C. Meneveau, R. Burns, S. Chen, A. Szalay, and G. Eyink, Journal of Turbulence p. N31 (2008).
[13] H. Yu, K. Kanov, E. Perlman, J. Graham, E. Frederix, R. Burns, A. Szalay, G. Eyink, and C. Meneveau, Journal of Turbulence (2012).
[14] G. B. Jeffery, Proc. R. Soc. A **102**, 161 (1922).
[15] M. Shin and D. L. Koch, J. Fluid Mech. **540**, 143 (2005).
[16] D. Vincenzi, J. Fluid Mech. (2013).
[17] B. Mehlig, M. Wilkinson, K. Duncan, T. Weber, and M. Ljunggren, Phys. Rev. E **72**, 051104 (2005).
[18] K. Gustavsson and B. Mehlig, Europhys. Lett.) **96**, 60012 (2011).
[19] K. Gustavsson and B. Mehlig, Phys. Rev. E **87**, 023016 (2013).
[20] M. S. Chong, A. E. Perry, and B. J. Cantwell, Phys. Fluids A: Fluid Dynamics **2**, 765 (1990).
[21] M. Chertkov, A. Pumir, and B. I. Shraiman, Phys. Fluids **11**, 2394 (1999).
[22] Z. S. She, E. Jackson, and S. A. Orszag, Nature **344**, 226 (1990).
[23] H. Brenner, Int. J. Multiphase Flow **1**, 195 (1974).